Eur. Phys. J. D **27**, 159–167 (2003)
DOI: 10.1140/epjd/e2003-00255-9

THE EUROPEAN PHYSICAL JOURNAL D

Light bullets from femtosecond filamentation

A. Couairon[a]

Centre de Physique Théorique, École Polytechnique[b], 91128 Palaiseau Cedex, France

Received 17 March 2003 / Received in final form 4 June 2003
Published online 12 August 2003

Abstract. A model for the propagation of femtosecond laser pulses in transparent media and the formation of light bullets is proposed. This model enable us to generalize Marburger's formula for the position of the nonlinear focus of the beam in the presence of delayed Kerr effect. It is shown that an instantaneous higher-order saturation tuned to mimic the defocusing effect due to the plasma generated by multiphoton ionization does not properly represent the dynamics of femtosecond filamentation as it violates causality and artificially promotes long distance propagation in the form of periodic oscillations around a spatial soliton. A causal description of multiphoton ionization leads to an extended moving focus model from which the formation of a synchronized structure exhibiting several focusing-defocusing cycles before eventual diffraction can be inferred.

PACS. 42.65.Sf Dynamics of nonlinear optical systems; optical instabilities, optical chaos and complexity, and optical spatio-temporal dynamics – 42.25.Bs Wave propagation, transmission and absorption – 42.65.Jx Beam trapping, self-focusing and defocusing; self-phase modulation – 52.38.Hb Self-focusing, channeling, and filamentation in plasmas

1 Introduction

Femtosecond laser pulses have been observed to self-channel in air over distances from several tenths to several hundred of meters [1–7]. This spectacular propagation forming narrow light filaments proceeds from the dynamical equilibrium between the conjugate effects of self-focusing, diffraction and ionization, which provides an efficient optical guiding mechanism for femtosecond pulses in gases [8–15,17]. Despite extensive investigations of self-focusing and self-trapping of intense laser beams for the last three decades [18–20], the question whether a spatial soliton supports the dynamics of the long range propagation of femtosecond laser pulses in the atmosphere is still open. From lightning protection [21] to light detection and ranging techniques [22–24], the applications of femtosecond filamentation request the transport of high intensities as light bullets [25–27] and therefore, this question is of crucial importance for the control of the propagation distance and the generic properties of light filaments.

The aim of this paper is twofold: first, we develop a nonlinear analysis leading to analytical self similar solutions of light filaments. It is based on the classical model equation governing the slowly varying envelope of the electric field coupled with an evolution equation for the density resulting from ionization [15,28,29]. Second, we show that these self-similar solutions constitute either spatial solitons or solutions oscillating globally around spatial solitons only when certain restrictive assumptions are made. In femtosecond filamentation in air, the defocusing effect of the plasma generated by multiphoton ionization and the delayed Kerr effect due to stimulated molecular Raman scattering induces a coupling between the forward and the backward parts of the pulse which influences its nonlinear dynamics. We show that when these effect are correctly taken into account, spatial solitons cannot form. In this case, our self-similar solutions constitute light bullets that closely follow the dynamics of the propagation of femtosecond laser pulses in transparent media. In particular, a short synchronized structure is formed and exhibits several focusing-defocusing cycles before final diffraction. This model constitutes an extended moving focus model [30] that we also compare with another model from the literature called the spatial replenishment model [9].

The outline of this paper is as follows. In Section 2, we briefly recall the model equations for the propagation of ultrashort laser pulses in air and we derive a partial differential equation for the beam waist radius, which fully describes the evolution of the filament in the form of a self-similar solution of the propagation equation. In Section 3, we generalize Marburger's formula for the position of the nonlinear focus of the beam in the presence of delayed Kerr effect. In Section 4, we show that an oversimplification of the model leads to a periodic pulse dynamics oscillating around a spatial soliton, which does not describe correctly femtosecond filamentation in air. In Section 5, we discuss multiphoton ionization and the delayed Kerr effect and we show that when causality is correctly

[a] e-mail: couairon@cpht.polytechnique.fr
[b] UMR 7644 du CNRS

accounted for in these effects, the main properties of femtosecond filamentation, including the formation of light bullets, are retained in our model. We finally compare this model to the moving focus [30] and the spatial replenishment models [9].

2 Model of femtosecond filamentation

We start from an extended paraxial model which describes the propagation along the z-axis of the linearly polarized laser pulse. The pulse is decomposed into a slowly varying amplitude and a carrier wave with frequency ω_0 and wavenumber $k \equiv n_0\omega_0/c$, where n_0 denotes the linear index of the medium, as $\mathbf{E} = \mathrm{Re}[\mathcal{E}\exp(\mathrm{i}kz - \mathrm{i}\omega_0 t_{lab})]\mathbf{e}_x$. The scalar envelope of the electric field $\mathcal{E}(x,y,z,t)$ evolves according to the nonlinear envelope equation [28] expressed in the reference frame moving at the group velocity $v_g \equiv \partial\omega/\partial k|_{\omega_0}$:

$$\frac{\partial\mathcal{E}}{\partial z} = \frac{\mathrm{i}}{2k}T^{-1}\left(\frac{\partial^2}{\partial x^2}+\frac{\partial^2}{\partial y^2}\right)\mathcal{E} - \mathrm{i}\frac{k''}{2}\frac{\partial^2}{\partial t^2}\mathcal{E} + \mathrm{i}k_0 n_2 T\left[(1-f)I(t) + f\int_{-\infty}^{t}\mathcal{R}(t-t')I(t')\mathrm{d}t'\right]\mathcal{E}(t) - \frac{\sigma}{2}(1+\mathrm{i}\omega_0\tau_c)\rho\mathcal{E} - \frac{\beta_K}{2}TI^{K-1}\mathcal{E}, \quad (1)$$

where $I \equiv |\mathcal{E}(x,y,z,t)|^2$, $\rho(x,y,z,t)$ denotes the electron density of the plasma generated by ionization and t refers to the retarded time variable $t_{lab} - z/v_g$. The first term on the right hand side (rhs) of equation (1) accounts for diffraction within the transverse plane. The second term accounts for group velocity dispersion with coefficient $k'' = 0.2$ fs^2/cm at 800 nm. The third and fourth terms on the rhs of equation (1) account for the Kerr effect with an instantaneous component due to the electronic response in the polarization and a delayed component, of fraction $f = 0.5$, due to stimulated molecular Raman scattering [31]. In air, at the laser wavelength $\lambda_0 = 800$ nm, the nonlinear index of refraction is $n_2 = 3.2\times10^{-19}$ cm^2/W and the critical power for self-focusing expresses as $P_{\mathrm{cr}} \equiv \lambda_0^2/2\pi n_0 n_2 = 3.2$ GW. The function

$$\mathcal{R}(t) = \exp(-t/\tau_{\mathrm{dK}})/\tau_{\mathrm{dK}} \quad (2)$$

mimics the molecular response of the gas with a characteristic time $\tau_{\mathrm{dK}} = 70$ fs. The fifth term on the rhs of equation (1) accounts for plasma absorption and defocusing. The cross-section for inverse Bremsstrahlung follows the Drude model [32] and reads $\sigma = k\omega_0\tau_c/n_0^2\rho_c(1+\omega_0^2\tau_c^2) = 5.1\times10^{-18}$ cm^2 with $\tau_c = 3.5\times10^{-13}$ s. In the limit $\tau_c \gg \omega_0^{-1}$, the defocusing term can be expressed as a function of the critical plasma density $\rho_c = 2\times10^{21}$ cm^{-3} above which the plasma becomes opaque: $k\sigma\omega_0\tau_c\rho \simeq k_0^2\rho/\rho_{\mathrm{c}}$. The last term in equation (1) accounts for energy absorption due to multiphoton ionization; the coefficient β_K is related to the multiphoton ionization rate. The operator $T \equiv 1 + \mathrm{i}\omega_0^{-1}\partial/\partial t$ accounts for space-time focusing and self-steepening of the pulse. It describes deviations from the slowly varying envelope approximation [15,28,29].

The generation of the plasma by multiphoton and avalanche ionization is described by the evolution equation for the electron density ρ

$$\partial\rho/\partial t = \sigma_K I^K(\rho_{\mathrm{at}} - \rho) + \eta\rho I. \quad (3)$$

For multiphoton ionization of oxygen molecules with the potential $U_i = 12.1$ eV, $K = 8$ photons are necessary to liberate an electron. The coefficient $\sigma_K = 3.7\times10^{-97}$ s^{-1} cm^{16} W^{-8} has been computed from Keldysh's theory [33] and is linked to β_K as $\beta_K = \sigma_K K\hbar\omega_0\rho_{\mathrm{at}}$, where $\rho_{\mathrm{at}} = 0.2\rho_{\mathrm{air}} = 5\times10^{18}$ cm^{-3} denotes the density of oxygen molecules. For avalanche ionization, $\eta = \sigma/U_i$. Unless otherwise specified, we will use these parameters and the input beams are modeled by collimated Gaussians with peak intensity I_0, a transverse waist $w_0 = 1$ mm, a temporal half width $t_p = 100$ fs, and an input peak power $P_{\mathrm{in}} = \pi w_0^2 I_0/2 = 10\,P_{\mathrm{cr}}$ ($I_0 = 2\times10^{12}$ W/cm^2):

$$\mathcal{E}(x,y,t,0) = \sqrt{I_0}\exp\left[-\left(x^2+y^2\right)/w_0^2 - t^2/t_p^2\right]. \quad (4)$$

In the following, we consider beams with cylindrical symmetry that retain this symmetry along propagation and we will use vector $\mathbf{r} = (x,y)$ for notational convenience. The analysis is therefore relevant for pulses with powers moderately above P_{cr} which do not lead to multifilamentation. Note, however, that it can be applied in the present form to high power pulses whenever they form a single filament.

The pulse power and the beam radius can be expressed as:

$$P(z,t) = \int I(\mathbf{r},z,t)\mathrm{d}\mathbf{r} \quad (5)$$

$$w^2(z,t) = \frac{1}{P(z,t)}\int r^2 I(\mathbf{r},z,t)\mathrm{d}\mathbf{r}. \quad (6)$$

From equation (1), we derive evolution equations for these quantities by means of the variational method developed by Anderson [34], or by applying the equivalent and more direct method proposed in [35]. The envelope of the electric field is expressed as a self similar (test) function

$$\mathcal{E}(\mathbf{r},z,t) = \mathcal{A}(z,t)\exp\left[-(1+\mathrm{i}\alpha(z,t))\xi^2 + \mathrm{i}\theta(z,t) - t^2/t_p^2\right] \quad (7)$$

where $\xi \equiv r/w(z,t)$, and $\mathcal{A}^2(z,t) = 2P(z,t)/\pi w^2(z,t)$. Then, it is introduced in integral equations derived from equation (1). The resulting set of equations for $\mathcal{A}$, α, θ, and w can then be combined to give equations for the pulse power and beam radius (see Ref. [35] and references therein for details). In the following, we discuss in detail the case where the power is preserved along propagation:

$$P(z,t) = P(z=0,t) = P_{\mathrm{in}}\exp\left(-t^2/t_p^2\right). \quad (8)$$

This is the case when only the main physical effects promoting femtosecond filamentation are considered, namely,

diffraction, self-focusing due to the Kerr effect and ionization which all preserve the pulse power. The propagation equation (1) then becomes

$$\frac{\partial \mathcal{E}}{\partial z} = \frac{\mathrm{i}}{2k}\left(\frac{\partial^2}{\partial r^2} + \frac{1}{r}\frac{\partial}{\partial r}\right)\mathcal{E} - \mathrm{i}\frac{k_0\rho}{2n_0\rho_c}\rho\mathcal{E} + \mathrm{i}k_0 n_2\left[(1-f)I(t) + f\int_{-\infty}^{t}\mathcal{R}\left(t-t'\right)I\left(t'\right)\mathrm{d}t'\right]\mathcal{E}(t). \quad (9)$$

Previous numerical simulations of equation (1) have shown that for the propagation of ultrashort laser pulses in air [15,17] and in silica glasses [36,37], the collapse occurring in a purely Kerr medium is arrested by multiphoton ionization. Other effects as, *e.g.*, group velocity dispersion can also arrest the collapse in principle [38,39]. This occurs, however, when the dispersion length $L_{\mathrm{GVD}} = t_p^2/2k''$ is comparable to the self-focusing length $L_{\mathrm{SF}} \sim z_R(P_{\mathrm{in}}/P_{\mathrm{cr}} - 1)^{-1/2}$ where $z_R = kw_0^2/2$ denotes the Rayleigh length. In air, unless large initial beams (promoting a weakly nonlinear self-focusing over extended distances) or beams with powers exceeding only slightly P_{cr} are used, the condition $L_{\mathrm{SF}} \sim L_{\mathrm{GVD}}$ is not fulfilled [40]. Group velocity dispersion is therefore neglected and similar reasons justify that multiphoton and plasma absorption, as well as space time focusing and self-steepening are neglected. We also neglect avalanche ionization prevailing for pulses longer than those considered here. All these effects may be reintroduced in the model later. Our aim is to determine, in these conditions, whether a spatial soliton can act as an attractor for the dynamics of long range propagation in the form of a light filament. The beam radius then satisfies

$$\frac{\partial^2 w}{\partial z^2} = \frac{4}{k^2 w^3}\left(1 + k^2 w^2 G\right), \quad (10)$$

where

$$G(z,t) = \int_0^\infty M(\xi,z,t)\left(1-2\xi^2\right)\mathrm{e}^{-2\xi^2}\mathrm{d}\xi^2, \quad (11)$$

$$M(\xi,z,t) = \frac{\rho(\xi,z,t)}{n_0^2\rho_c} - 2\frac{n_2}{n_0}\left[(1-f)I(\xi,z,t) + f\int_{-\infty}^{t}R\left(t-t'\right)I\left(\xi,z,t'\right)\mathrm{d}t'\right]. \quad (12)$$

After performing the various integrations in equations (11, 12), we obtain the evolution equation for the beam radius:

$$\frac{k^2w^3}{4}\frac{\partial^2 w}{\partial z^2} = 1 - \frac{P_{\mathrm{in}}}{P_{\mathrm{cr}}}\left[(1-f)\mathrm{e}^{-2(t/t_p)^2} - 4fw^4\int_{-\infty}^{t}\frac{\mathcal{R}\left(t'-t\right)\exp\left(-2t'^2/t_p^2\right)}{\left(w'^2+w^2\right)^2}\mathrm{d}t'\right] + \mu w_0^{2K-2}w^4\int_{-\infty}^{t}\frac{\exp\left(-2K\left(t'/t_p\right)^2\right)}{\left(w'^2+Kw^2\right)^2 w'^{2K-2}}\mathrm{d}t', \quad (13)$$

where $\mu \equiv 2Kk_0z_R\rho_0/\rho_c$, $z_R \equiv kw_0^2/2$ is the Rayleigh length, $\rho_0 \equiv \sigma_K\rho_{\mathrm{at}}I_0^K$, $w \equiv w(z,t)$ and $w' \equiv w(z,t')$. Note that equation (13) is obtained by keeping the variation of $w'(z,t')$ with time in the electron density $\rho \sim \int_{-\infty}^{t}\sigma_K\rho_{\mathrm{at}}[2P_{\mathrm{in}}/\pi w(z,t')]^K\exp(-2K\xi'^2)\mathrm{d}t'$, where $\xi'^2 = r^2/w'^2(z,t')$ and by transforming ξ' as $\xi'^2 = \xi^2w^2(z,t)/w'^2(z,t')$ in the integration over the transverse spatial coordinate. Equation (13) therefore differs from that obtained in [35] for the beam radius, and in other works relying on variational analysis [41–43]. Below, we discuss in details the consequences for the physics of femtosecond pulse propagation these differences imply.

The pulse is stacked into temporal slices, each of which containing a power given by equation (8). Equation (13) constitutes a dynamical system that can be viewed as a continuous set of coupled differential equations for the radii of the various temporal slices in the pulse. Each slice evolves as an oscillator in a pseudo-potential, which does not only vary with w, but also with time through the coupling by the electron plasma density and the delayed Kerr effect. Before discussing numerical solutions of equation (13), some insight obtained from direct inspection of this equation will be given.

3 Position of the nonlinear focus of the beam in the presence of delayed Kerr effect

First, we discuss the case when only the Kerr effect is taken into account, *i.e.*, no plasma generation occurs as in the initial self-focusing stage. Equation (13) with $\mu = 0$ describes how the radii shrink in the transverse diffraction plane under the action of both instantaneous and delayed components in the Kerr effect. An expression for the position of the nonlinear focus may be obtained by assuming an expansion in time of the radius, *i.e.*, $w' \sim w + \mathrm{h.o.t.}$ where h.o.t. denotes a higher order term that is neglected (see below for a discussion of this approximation). Equation (13) can then be integrated as

$$w^2(z,t) = w_0^2 - \left(\frac{\tilde{P}_{\mathrm{in}}(t)}{P_{\mathrm{cr}}} - 1\right)\frac{z^2}{z_R^2} \quad (14)$$

where

$$\tilde{P}_{\mathrm{in}}(t) = P_{\mathrm{in}}\left[(1-f)\mathrm{e}^{-2t^2/t_p^2} + f\int_{-\infty}^{t}\mathcal{R}(t'-t)\mathrm{e}^{-2\left(t'/t_p\right)^2}\mathrm{d}t'\right]. \quad (15)$$

From the expression of the input power given by equation (8) and the fact that the pulse power is preserved for each temporal slice, the slices with power above P_{cr} are contained in $[-t^*, t^*]$ where $t^* = \sqrt{0.5\log(P_{\mathrm{in}}/P_{\mathrm{cr}})}$. Equation (14), however, shows that the slices that undergo a compression due to both contributions of the Kerr effect are such that $\tilde{P}_{\mathrm{in}}(t) > P_{\mathrm{cr}}$. Due to the delayed component in the Kerr effect, the time domain where this condition is

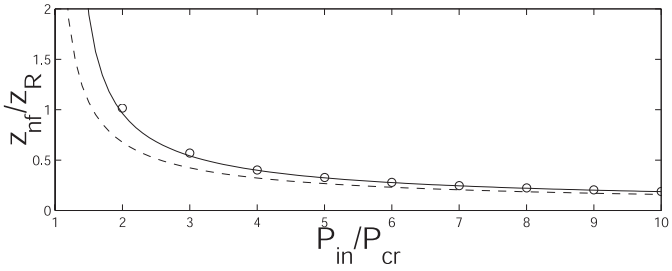

Fig. 1. Position of the nonlinear focus as a function of $P_{\rm in}/P_{\rm cr}$ from equation (18) (solid line), and from numerical simulations of equation (1) (circles). Marburger's result is shown in dashed line.

satisfied is shorter than $[-t^*, t^*]$. This leads to the definition of an effective critical power $P_{\rm cr}^{\rm eff} = P_{\rm in}\exp(-t^{\dagger 2}/t_p^2)$ where $t^\dagger$ is the smallest value such that $\tilde{P}_{\rm in}(t^\dagger) = P_{\rm cr}$, and for future reference, t^+ is the largest.

Each time slice for which $t^\dagger < t < t^+$ undergoes a transverse compression that ends in a collapse singularity on the propagation axis. The location of the collapse for the time slice t then reads as

$$z_c(t) = \frac{z_R}{\sqrt{\tilde{P}_{\rm in}(t)/P_{\rm cr} - 1}}. \tag{16}$$

The whole pulse therefore collapse at the shortest of these distances which constitutes a good approximation for the position $z_{\rm nf}$ of the nonlinear focus of the beam reached when a nonlinear effect such as ionization saturates the collapse

$$z_{\rm nf} = \frac{z_R}{\sqrt{\max_t \tilde{P}_{\rm in}(t)/P_{\rm cr} - 1}}. \tag{17}$$

Equations (17, 15) constitute a generalization of the equivalent formula valid for self-focusing by instantaneous Kerr effect only, with $\tilde{P}_{\rm in} = P_{\rm in}$ [44]. We conjecture that a best fit for the position of the nonlinear focus may be obtained by generalizing Marburger's formula [45] as

$$z_{\rm nf} = \frac{z_R}{2.725\sqrt{[(\max_t \tilde{P}_{\rm in}(t)/P_{\rm cr})^{1/2} - 0.852]^2 - 0.0219}}. \tag{18}$$

Figure 1 shows the position of the nonlinear focus obtained by numerical simulations of equation (18) as a function of $P_{\rm in}/P_{\rm cr}$ (circles). Equation (18) is shown in solid curve and despite the approximation made, it is in quite good agreement with the numerical data with less than 1% error on the position of the nonlinear focus for $P_{\rm in}/P_{\rm cr} \geq 3$. For comparison, Marburger's formula is retrieved for $\tilde{P}_{\rm in}(t) = P_{\rm in}$ in equation (18) and is shown in dashed curve. It underestimates the position of the nonlinear focus when a fraction of the Kerr effect is delayed as in air. In the presence of delayed Kerr effect, the position of the nonlinear focus is therefore correctly approximated by the couple of equations (15, 18), which is a simple extension of Marburger's formula.

4 Simplified model with Kerr effect and instantaneous multiphoton ionization

Second, we take into account plasma defocusing in equation (13) while keeping the approximation $w' \sim w + \text{h.o.t.}$ in the integrals and neglecting the higher order terms. Equation (13) then becomes

$$\frac{\partial^2 w}{\partial z^2} = \frac{4}{k^2}\left(\frac{1}{w^3}(1 - \frac{\tilde{P}_{\rm in}(t)}{P_{\rm cr}}) + \frac{c(t)}{w^{2K+1}}\right), \tag{19}$$

where $\tilde{P}_{\rm in}$ is given by equation (15) and

$$c(t) = \mu w_0^{2K-2}\frac{1}{2(K+1)^2}\sqrt{\frac{\pi}{2K}}\left[1 + \mathrm{erf}\left(\sqrt{2K}t/t_p\right)\right]. \tag{20}$$

Physically, the assumption made means that each temporal slice evolves independently: it amounts to relaxing the physical coupling between the temporal slices. In the terms accounting for the delayed Kerr effect and plasma defocusing in the simplified model (19), a time asymmetry between the leading and the trailing part of the pulse is kept; it does not, however, replace the physical coupling between the slices that these effects induce. In equation (19), plasma defocusing for example, is replaced by a saturation, still occurring on the trail of the pulse due to the time asymmetry, but with a level depending on the local intensity only and not on the intensity of the leading part of the pulse as should be the case in order to keep the model causal. Causality is broken similarly in the term corresponding to the delayed Kerr effect. In spite of this limitation, we will briefly discuss the solutions of this simplified model in order to compare the results with those of the complete model (13) and show that this approximation for the saturating nonlinearity leads to a pulse dynamics that cannot correctly describe femtosecond filamentation. This point is important since, due to its simplicity, this approximation is used in most of the applications of the variational methods to femtosecond filamentation and in some numerical models in the literature.

The solutions of equation (19) for $w(z,t)$ can be easily found by considering the mechanical analogy with a continuous set of particles with positions $w(z,t)$, moving in the potential

$$V(w,t) = \frac{2}{k_0^2}\left[\frac{1}{w^2}\left(1 - \frac{\tilde{P}_{\rm in}(t)}{P_{\rm cr}}\right) + \frac{c(t)}{Kw^{2K}}\right] \tag{21}$$

where z plays the role of time for the motion of the particles, and t refers to a given particle. Figure 2a shows the potentials (21) as functions of w for various temporal slices. There is no equilibrium solution for the temporal slices containing a subcritical power, *i.e.*, such that $\tilde{P}_{\rm in}(t) < P_{\rm cr}$. For these slices diffraction prevails.

In the domain $[-t^\dagger, t^+]$, there is an equilibrium solution corresponding to the minimum of the potential (21), given by

$$w_{\rm eq}^2(t) = \left(\frac{c(t)}{\frac{\tilde{P}_{\rm in}(t)}{P_{\rm cr}} - 1}\right)^{1/(K-1)}. \tag{22}$$

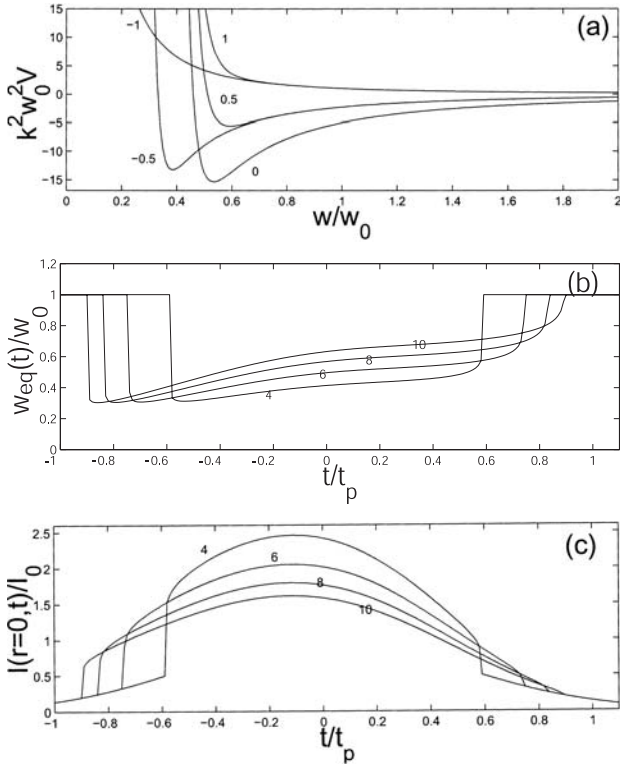

Fig. 2. (a) Potential as a function of beam radius for the temporal slices $t/t_p = -1$, -0.5, 0, 0.5 and 1.5. (b) Radius and (c) temporal shapes of the spatial solitons defined by (22), for the values of $P_{\rm in}/P_{\rm cr}$ indicated on the curves.

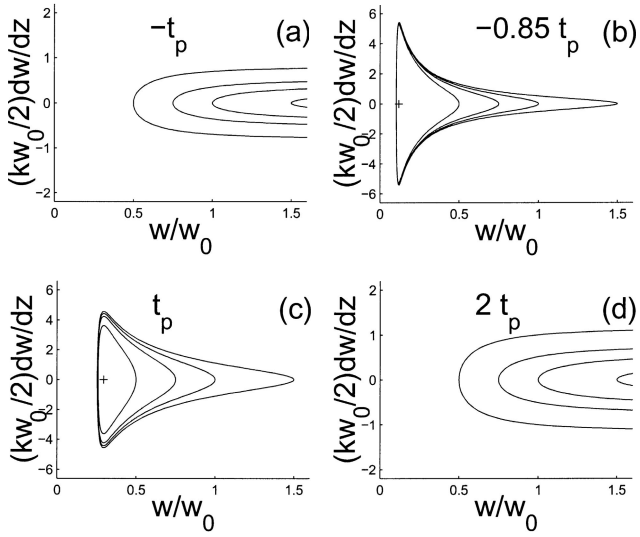

Fig. 3. Phase portraits of equation (19) with $P_{\rm in} = 10P_{\rm cr}$ for the time slices (a) $t = -t_p$, (b) $t = -0.85t_p$, (c) $t = 0.85t_p$ and (d) $t = 2t_p$.

This quantity is plotted in rescaled coordinates in Figure 2b for various values of $P_{\rm in}/P_{\rm cr}$ indicated on the curves, varying from 4 to 10. The corresponding pulse shape is plotted in Figure 2c. Here w_0 corresponds to the waist of the Gaussian beam with the same input power. We have kept this value constant in the feet of these pulses which rise and fall off abruptly around $t^\dagger$ and t^+. Their narrowest part is located immediately behind $t^\dagger$. The radius of these solutions slightly increases with time but the pulses are globally narrower in their central part than in their feet, in contrast with a Gaussian pulse that has a constant in time radius. Within the framework of this model, these pulses represent the closest solutions to spatial solitons as they exhibit a narrow and steady radius in their central part while only their feet diffract.

Other solutions different from (22) are presented on the phase portraits of equation (19) in Figure 3. Each phase portrait corresponds to a given time slice indicated above the trajectories which follow increasing z. Figure 3a is typical of the time slices $t < t^\dagger$. When a focusing lens is used, the initial condition satisfies $\mathrm{d}w/\mathrm{d}z(z = 0, t) < 0$ and the radius initially decreases for each slice but eventually increases under the action of diffraction. The phase portraits for the time slices $t > t^+$ are similar [see Fig. 3d] except that the radii not only increase because of diffraction but also because of the defocusing effect of the plasma. Figures 3b and 3c correspond to the central part of the pulse with $t^\dagger < t < t^+$. The trajectories oscillate around the fixed points shown with a + sign. The set of these fixed points for all t constitutes the spatial soliton with radii given by (22). The cycles reflect the interplay between self-focusing (part $\mathrm{d}w/\mathrm{d}z < 0$ of the cycles) and plasma defocusing (part $\mathrm{d}w/\mathrm{d}z < 0$). The oscillation period $Z(t)$ depends on the time slice only and is not correlated to the dynamics of the neighboring time slices. From this model, the pulse exhibits an oscillatory behavior but the global dynamics is not synchronized. The oscillation period is shown in Figure 6 (thin curve) as a function of time for the trajectory with $w(z = 0, t) = w_0$. It is longer for the slices in the trail and the leading edge of the pulse than for the central slices. As a result a pulse with initially synchronized slices, as *e.g.*, a Gaussian input pulse with $w(z = 0, t) = w_0$ for all t will slowly loose this synchronism along propagation, and finally exhibit a multipeaked structure with various maxima corresponding to the slices that arrive nearly simultaneously at the end of a focusing half-cycle. Figure 4 shows this behavior for a pulse with $P_{\rm in} = 10P_{\rm cr}$. The pulse intensity on the propagation axis $r = 0$ is plotted in thin lines as a function of time for various propagation distances (thick curves refer to the solutions of Eq. (13) and will be discussed in the next section). Two peaks are formed at $z = 0.5z_R$ [Fig. 3b] from the initially Gaussian pulse. At $z = z_R$ [Fig. 3c], the leading peak hidden by the thick curve evolves slowly while the central maximum near $t = 0$ is in a self-focusing process. Between $z = z_R$ and $z = 1.3z_R$, the central maximum forms a spiky structure and a third peak develops in the trail resulting in a multipeaked temporal structure [Fig. 3d]. It goes without saying that the number of subpulses increases along propagation and is all the larger as the ratio $P_{\rm in}/P_{\rm cr}$ is large.

Although these temporal profiles may seem close to those obtained in numerical simulations of equation (1) [15,16], it should not be forgotten that the oscillating behavior in this model is fully determined by

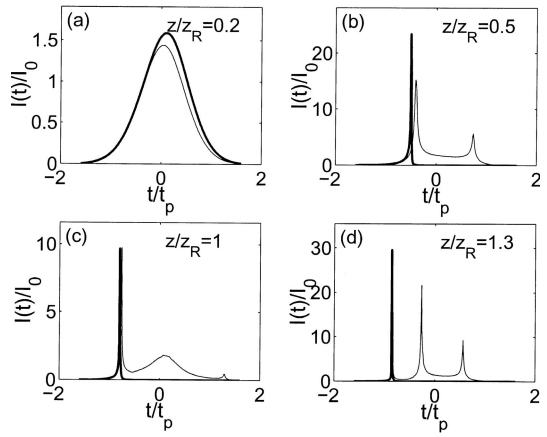

Fig. 4. Pulse intensity as a function of time computed from model (19) (thin curves) and from model (13) at the propagation distances (a) $z = 0.2z_R$, (b) $z = 0.5z_R$, (c) $z = z_R$ and (d) $z = 1.3z_R$.

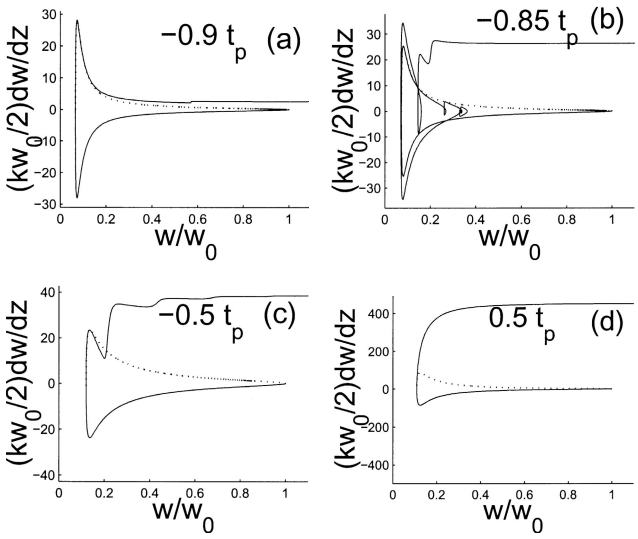

Fig. 5. Numerically determined phase portraits for equation (13) and $P_{\rm in} = 10P_{\rm cr}$. (a) $t = -0.9t_p$; (b) $t = -0.85t_p$; (c) $t = -0.5t_p$; (d) $t = 0.5t_p$. The dots indicate the trajectory that would be followed if the solutions were periodic.

the fact that the coupling between the various temporal slices is neglected. Note the analogy of this model with the crude assumption of an instantaneous ionization which amounts to replacing the plasma density in equation (1) by $\rho \sim \sigma_K \rho_{\rm at} t_p I^K(\mathbf{r}, z, t)$. This approximation does not respect causality and does not even preserve the asymmetry between the forward and the backward part of the pulse. The model equation (19), with a constant $c(t) = c(\infty)$ relies on the same approximation. In this way, a global oscillating dynamics is forced around the spatial soliton defined by equation (22) with $c(t) = c(\infty)$. Therefore, any numerical model with this non causal saturation term for multiphoton ionization cannot correctly describe the nonlinear dynamics of femtosecond filamentation as it amounts to assuming *a priori* an oscillatory dynamics around a spatial soliton. A correct model should allow the possibility of oscillating behaviors but not contain an intrinsically periodic behavior.

5 Extended moving focus model

When the coupling between the various time slices is taken into account as in equation (13), each time slice can still be viewed as an oscillator but the pulse forms now a continuous set of *coupled* oscillators and its global dynamics significantly differs from that resulting from equation (19). The coupling between the various time slices arises from the integral terms, *i.e.* from the delayed Kerr effect and plasma defocusing. The coupling is weak for negative times and becomes effective for sufficiently large t. The delayed Kerr effect indeed acts on the trail and the electron plasma also saturates self-focusing on the trail of the pulse. Here the saturation, however, also depends on the dynamics of the pulse in its leading edge. This model therefore does not violate causality in contrast with equation (19) and with numerical models with an instantaneous ionization as, *e.g.*, equation (1) with $\rho \sim \sigma_K \rho_{\rm at} t_p I^K(\mathbf{r}, z, t)$.

The pulse dynamics resulting from this model will be discussed from the phase portraits of the dynamical system (13) that must be computed numerically. Starting from Gaussian initial pulses with $w(z = 0, t) = w_0$, equation (13) is integrated by increasing the time coordinate from $t = -\infty$ for each position z so as to take into account the effect of the leading slices on the subsequent slices. The solutions are displayed in Figure 5 in the form of partial phase portraits $(w(z,t), \partial w/\partial z)$ for four different time slices. In contrast with Figure 3 where the trajectories corresponding to initial Gaussian pulses with different waists were displayed, only one trajectory (defined by $w(z = 0, t) = w_0$) per phase portrait is shown in Figure 5 for the sake of clarity. In a given phase portrait, this trajectory can indeed cross the trajectories defined by other initial values because of the coupling that links the time slices to their neighbors. It can also intersect itself since only projections of the phase space $(w, \partial w/\partial z, z)$ are actually shown for each time slice in Figure 5.

The effective critical power for self-focusing refers to the power of the time slice for which a transition occurs from a phase portrait similar to Figure 3a (for a time slice with subcritical power, the trajectory starting from $w(z = 0) = w_0$, $\mathrm{d}w/\mathrm{d}z = 0$ has increasing w and positive $\mathrm{d}w/\mathrm{d}z$ indicating diffraction), to a phase portrait exhibiting an initial focusing stage with $\mathrm{d}w/\mathrm{d}z < 0$ as in Figures 3b and 5a. We will keep the notations $t^\dagger$ and t^+ for the time slices with power equal to the effective critical power for self-focusing although these values differ from those defined in Section 4 from equation (19). The phase portraits corresponding to the central slices of the pulse ($t^\dagger < t < t^+$) with power above the effective critical power for self-focusing are shown in Figures 5a–5d. In contrast with the solutions of (19), the trajectories are neither closed, nor do they all exhibit complete focusing–defocusing cycles. Closed trajectories shown in dotted curves would be periodic. As indicated by the loops in Figure 5b, some temporal slices located in the forward

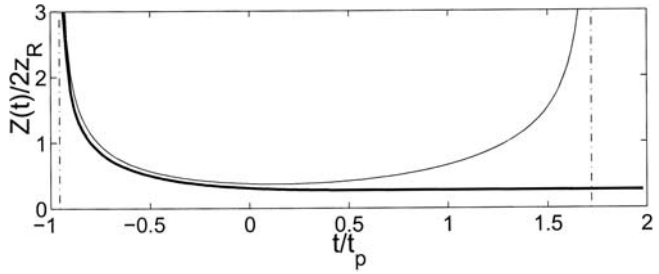

Fig. 6. Oscillation period from model (19) (thin line) and duration of the initial focusing cycle from (13) (thick line).

part of the pulse exhibit a nearly periodic behavior; they may undergo several focusing–defocusing cycles before an eventual diffraction stage. Figures 5c and 5d are typical of the temporal slices in the center and in the trail of the pulse with $t < t^+$. After a single focusing half-cycle, these slices are defocused without oscillations of their diameter. In this model, periodic oscillations of the beam diameter are therefore not assumed *a priori* as in equation (19). Figure 5b shows that a finite number of oscillations may occur for some slices. Oscillations may not only happen in the forward part, but also in the trail of the pulse, although only the leading part oscillates in the example of Figure 5. Multipeaked structures for the pulse intensity are generically formed along propagation because the oscillating temporal slices of the pulse have different pseudo-periods. The duration of a focusing-defocusing cycle for a slice located in the trail indeed depends on the dynamics of the pulse slices located in the leading edge, and therefore on the propagation distance. This constitutes one of the main difference between model (19) and model (13).

Figure 6 shows the oscillation half-period for the radii of the temporal slices in the central part of the pulse for model (19) (thin curve) and the duration of the initial focusing half-cycle for model (13), *i.e.*, the distance requested by each slice to reach its minimal radius. For the forward part of the pulse with negative times, the duration of the first focusing stage is nearly equal to half the oscillation period for the pulse radius obtained from equation (19). For equation (13), the trailing slices are synchronized whereas for equation (19), the oscillation period is longer in the trail and in the leading part than in the central part. As a result, in model (13), the nonlinear focii for the trailing slices are located at the same position on the z-axis. The first part of the filament immediately behind the nonlinear focus of the beam can be viewed as the collection of the various focii on the propagation axis, but mainly the leading slices in the pulse prevail in this moving focus. Beyond these primary focii, the filament can be viewed as the collection of secondary focii on the propagation axis, corresponding to the successive focii of the oscillating slices (which are the leading slices in the example of Fig. 5).

The evolution of the pulse temporal profile is shown in thick curves in Figure 4. The central and trailing slices are focused over a distance roughly equal to $0.3z_R$. Then, these slices are defocused while the leading slices around $-0.85t_p$ make several oscillations over a longer distance, resulting in a spiky temporal profile shown in Figures 4b–4d. Here, a temporal profile with a single peak is obtained for $P_{\rm in} = 10P_{\rm cr}$. As for light bullets, its duration is ultrashort and it possesses long range propagation properties since the focus of the leading slice already exceeds the position of the nonlinear focus by more than three Rayleigh lengths. Multipeaked structure can also arise from this model but do not result from the assumption of a periodic dynamics as in equation (19). Preliminary studies have shown that when power losses arising from multiphoton absorption and from the self-steepening effect are taken into account in the model, multipeaked structure are more easily formed at the same input power.

Although a global periodic behavior is not *a priori* assumed in this model, oscillatory behaviors with a finite number of cycles are not precluded because of the presence of oscillating slices in the pulse. Note that the difference between the distance over which these focusing-defocusing cycles occur and the distance to the nonlinear focus of the beam (first self-focusing cycle) determines the length of the filament. In this model no energy losses were considered and the length of the filament is however finite. Energy losses are important to precisely quantify the length of a filament but the long range propagation of femtosecond laser pulses in the form of a filament mainly relies on the physical effects ensuring the focusing and defocusing properties of the beam. Energy losses only bounds the filamentation length obtained from this dynamical equilibrium.

Ideally, in the framework of this model a spatial soliton would be constituted by a set of fixed points of (13) satisfying $\partial w/\partial z = 0$ and $\partial^2 w/\partial z^2$ for all t. It is clearly impossible to find such a set of fixed points for subcritical slices, except if $w(t) = \infty$ for $t < t^\dagger$ and $t > t^+$. Applying these conditions, we have sought for a solution in the central slices $t^\dagger < t < t^+$, by solving numerically equation (13) with $\partial^2 w/\partial z^2 = 0$, but only very localized solutions (shorter than $10^{-2}t_p = 1$ fs) could be found. These light bullets are close to the temporal profiles shown in thick curves in Figures 4b–4d, but the question whether they constitute attractors for the dynamics of equation (1) is still open.

To conclude we will briefly compare our interpretation of femtosecond filamentation inferred from model (13) with previous models. The model we have proposed is nothing else than an extended moving focus model that takes into account the defocusing effect of the plasma generated by multiphoton ionization and the delayed component in the Kerr effect. In this respect, it extends the model proposed in [30] relying on instantaneous Kerr effect and diffraction, *i.e.*, with a validity range limited to the self-focusing stage before the nonlinear focus. According to the original picture of the moving focus model given in [30], a beam focused by a lens cannot form a femtosecond filament beyond the linear focus of the lens; experimental results were shown to be in contradiction with this model [46]. When the coupling due to multiphoton ionization is carefully taken into account as in equation (13),

the formation of a filament beyond the linear focus of a lens is explained by the fact that the distance covered by the focusing-defocusing cycles of the oscillating slices is larger than the focal length. This clearly happens when the focal length is smaller than the Rayleigh length.

The present model also explains the occurrence of multipeaked structures commonly obtained in numerical simulations of equation (1) [15]. In this respect, it can be viewed as a quantitative version of another famous model called the spatial replenishment model (SRM) [9]. The SRM interprets qualitatively the physics of femtosecond pulse propagation from the results of numerical simulations of equation (1). Two important differences remain, however, between this model and the SRM: (i) the SRM relies on the extinction of the leading peak of the pulse to make the replenishment possible [47]. The decay of the leading peak was observed numerically and may have been induced by any effect in equation (1) that promotes a reduction of the power contained in the leading peak, such as multiphoton absorption, group velocity dispersion or other losses. No losses are considered in the present model, yet, a decay of the leading peak occurs when the focusing of the trailing part of the pulse is delayed by a half focusing-defocusing cycle for the leading peak, which happens for powers exceeding moderately the critical power (this is the case of the numerical results on the spatial replenishment model). (ii) The SRM correctly describes the formation of ring patterns in the intensity distribution. The present model assumes a self-similar Gaussian function in the transverse diffraction plane. In spite of this limitation, the model retains the oscillating dynamics of the pulse propagation which is therefore not inherent to the ring formation. The model can even be applied to different, non-Gaussian test functions in order to predict correctly the occurrence of these ring patterns. Although a complete development of this analysis is beyond the scope of the present paper, the main steps to follow are briefly discussed below. For a test function $\phi(z, r/w(z))$, we define a new beam radius $W(z,t)$ linked to the mean square radius $w(z,t)$ by:

$$W^2(z,t) = w^2(z,t)\frac{\int \xi^2\phi^2(z,\xi)\mathrm{d}\xi^2}{\int \phi^2(z,\xi)\mathrm{d}\xi^2}, \tag{23}$$

where $\xi \equiv r/w(z)$. The generalization of equation (13) then reads as

$$\begin{aligned}\frac{k^2W^3}{4}\frac{\partial^2 W}{\partial z^2} = \mathcal{D}(z) - \frac{P_{\mathrm{in}}}{P_{\mathrm{cr}}}\Bigg[&(1-f)\mathcal{F}(z)\mathrm{e}^{-2(t/t_p)^2} \\ &- 4f\mathcal{G}(z)W^2\int_{-\infty}^{t}\frac{\mathcal{R}(t'-t)\mathrm{e}^{-2(t'/t_p)^2}}{W(z,t')^2} \\ &\times\int_0^{+\infty}\phi^2\left(\xi\frac{W(z,t)}{W(z,t')}\right)\left(2+\xi\frac{\partial}{\partial\xi}\right)\phi^2(z,\xi)\mathrm{d}\xi^2\Bigg] \\ &+ \mu w_0^{2K-2}\mathcal{I}(z)W^2\int_{-\infty}^{t}\frac{\mathrm{e}^{-2K\left(t'/t_p\right)^2}}{W^{2K}(z,t')} \\ &\times\int_0^{+\infty}\phi^{2K}\left(\xi\frac{W(z,t)}{W(z,t')}\right)\left(2+\xi\frac{\partial}{\partial\xi}\right)\phi^2(z,\xi)\mathrm{d}\xi^2 \end{aligned} \tag{24}$$

$$\mathcal{D}(z) = \frac{\left(\int\left(\partial\phi/\partial\xi\right)^2\mathrm{d}\xi^2\right)\left(\int\xi^2\phi^2(z,\xi)\mathrm{d}\xi^2\right)}{\left(\int\phi^2(z,\xi)\mathrm{d}\xi^2\right)^2} \tag{25}$$

$$\mathcal{F}(z) = 4\frac{\left(\int\phi^4(z,\xi)\mathrm{d}\xi^2\right)\left(\int\xi^2\phi^2(z,\xi)\mathrm{d}\xi^2\right)\left(\int\phi^2(0,\xi)\mathrm{d}\xi^2\right)}{\left(\int\phi^2(z,\xi)\mathrm{d}\xi^2\right)^3} \tag{26}$$

$$\mathcal{G}(z) = 2\frac{\left(\int\xi^2\phi^2(z,\xi)\mathrm{d}\xi^2\right)\left(\int\phi^2(0,\xi)\mathrm{d}\xi^2\right)^2}{\left(\int\phi^2(z,\xi)\mathrm{d}\xi^2\right)^3} \tag{27}$$

$$\mathcal{I}(z) = \frac{2^K}{K}\frac{\left(\int\xi^2\phi^2(z,\xi)\mathrm{d}\xi^2\right)^K\left(\int\phi^2(0,\xi)\mathrm{d}\xi^2\right)^{K+1}}{\left(\int\phi^2(z,\xi)\mathrm{d}\xi^2\right)^{2K+1}}\cdot \tag{28}$$

Once a test function is chosen, the evolution of the mean square radius $w(z,t)$ as a function of the propagation distance follows from equation (23) and the integration of equation (24). With a Gaussian $\phi(z,\xi) = \exp(-\xi^2)$, equation (24) coincides with equation (13). A test function allowing ring formation reads as $\phi(z,\xi) = (\exp(-(\xi - d(z))^2) + \exp(-(\xi + d(z))^2)$, where $d(z)$ is the normalized distance of the ring to the propagation axis. Equation (24) applied to this test function preserves the dynamics of the extended moving focus model obtained above with the Gaussian test function while it is likely to reproduce the rings formed by defocusing of the central part in the trail of the pulse, as shown in the spatial replenishment model [9].

Finally, the physical effects that induce power losses, such as multiphoton and plasma absorption, group velocity dispersion, space-time-focusing and pulse self-steepening can modify the dynamics of the light bullets identified in this model. Whether these effects induce a relaxation to a stable spatial soliton promoting a propagation over a longer distance or merely consume the pulse energy and therefore reduce the filamentation length is still an open question that belong to the perspectives of the present study.

Fruitful and stimulating discussions with A. Mysyrowicz, M. Franco, B. Lamouroux, G. Méchain, B. Prade and S. Tzortzakis are gratefully acknowledged.

References

1. A. Braun, G. Korn, X. Liu, D. Du, J. Squier, G. Mourou, Opt. Lett. **20**, 73 (1995)
2. E.T.J. Nibbering, P.F. Curley, G. Grillon, B.S. Prade, M.A. Franco, F. Salin, A. Mysyrowicz, Opt. Lett. **21**, 62 (1996)
3. B. La Fontaine, F. Vidal, Z. Jiang, C.Y. Chien, D. Comtois, A. Desparois, T.W. Johnston, J.-C. Kieffer, H. Pépin, Phys. Plasmas **6**, 1615 (1999)
4. J. Schwarz, P. Rambo, J.-C. Diels, M. Kolesik, E.M. Wright, J.V. Moloney, Opt. Commun. **180**, 383 (2000)
5. S. Tzortzakis, B. Lamouroux, A. Chiron, M. Franco, B.S. Prade, A. Mysyrowicz, S.D. Moustaizis, Opt. Lett. **25**, 1270 (2000)

6. S. Tzortzakis, B. Lamouroux, A. Chiron, S.D. Moustaizis, D. Anglos, M. Franco, B. Prade, A. Mysyrowicz, Opt. Commun. **197**, 131 (2001)
7. D. Mikalauskas, A. Dubietis, R. Danielus, Appl. Phys. B **75**, 899 (2002)
8. V.P. Kandidov, O.G. Kosareva, S.A. Shlenov, Quant. Electron. **24**, 905 (1994)
9. M. Mlejnek, E.M. Wright, J.V. Moloney, Opt. Lett. **23**, 382 (1998)
10. M. Mlejnek, E.M. Wright, J.V. Moloney, Opt. Expr. **7**, 223 (1999)
11. M. Mlejnek, M. Kolesik, J.V. Moloney, E.M. Wright, Phys. Rev. Lett. **83**, 2938 (1999)
12. A. Chiron, B. Lamouroux, R. Lange, J.-F. Ripoche, M. Franco, B. Prade, G. Bonnaud, G. Riazuelo, A. Mysyrowicz, Eur. Phys. J. D **6**, 383 (1999)
13. J.V. Moloney, M. Kolesik, M. Mlejnek, E.M. Wright, Chaos **10**, 559 (2000)
14. M. Nurhuda, A. Suda, M. Hatayama, K. Nagasaka, K. Midorikawa, Phys. Rev. A **66**, 023811 (2002)
15. A. Couairon, S. Tzortzakis, L. Bergé, M. Franco, B. Prade, A. Mysyrowicz, J. Opt. Soc. Am. B **19**, 1117 (2002)
16. A. Couairon, L. Bergé, Phys. Rev. Lett. **88**, 135003 (2002)
17. A. Couairon, Phys. Rev. A **68**, 015801 (2003)
18. R.Y. Chiao, E. Garmire, C.H. Townes, Phys. Rev. Lett. **13**, 479 (1964)
19. J.H. Marburger, E. Dawes, Phys. Rev. Lett. **21**, 556 (1968)
20. V.I. Bespalov, V.I. Talanov, JETP Lett. **3**, 307 (1966)
21. F. Vidal, D. Comtois, C.-Y. Chien, A. Desparois, B. La Fontaine, T.W. Johnston, J.-C. Kieffer, H.P. Mercure, F.A. Rizk, IEEE Trans. Plasma Sci. **28**, 418 (2000)
22. L. Wöste, C. Wedekind, H. Wille, P. Rairoux, B. Stein, S. Nikolov, C. Werner, S. Neirdeimer, F. Ronneberger, H. Schilinger, R. Sauerbrey, Las. Optoelectr. **29**, 51 (1997)
23. P. Rairoux, H. Schillinger, S. Neirdeimer, M. Rodriguez, F. Ronneberger, R. Sauerbrey, B. Stein, D. Waite, C. Wedekind, H. Wille, L. Wöste, C. Ziener, Appl. Phys. B **71**, 573 (2000)
24. E. Frejafon, J. Kasparian, P. Rambaldi, B. Vezin, V. Boutou, J. Yu, M. Ulbricht, D. Weidauer, B. Ottobrini, E. de Saeger, B. Krämer, T. Leisner, P. Rairoux, L. Wöste, J.-P. Wolf, Eur. Phys. J. D **4**, 231 (1998)
25. Y. Silberberg, Opt. Lett. **15**, 1282 (1990)
26. P. Goorjian, Y. Silberberg, J. Opt. Soc. Am. B **14**, 3253 (1997)
27. J.X. Xin, Physica D **135**, 345 (2000)
28. T. Brabec, F. Krausz, Phys. Rev. Lett. **78**, 3282 (1997)
29. A.L. Gaeta, Phys. Rev. Lett. **84**, 3582 (2000)
30. A. Brodeur, C.Y. Chien, F.A. Ilkov, S.L. Chin, O.G. Kosareva, V.P. Kandidov, Opt. Lett. **22**, 304 (1997)
31. J.F. Ripoche, G. Grillon, B.S. Prade, M.A. Franco, E. Nibbering, H.R. Lange, A. Mysyrowicz, Opt. Commun. **135**, 310 (1997)
32. E. Yablonovitch, N. Bloembergen, Phys. Rev. Lett. **29**, 907 (1972)
33. L.V. Keldysh, ZhETF **47**, 1945 (1964); Sov. Phys. JETP **20**, 1307 (1965)
34. D. Anderson, M. Bonnedal, Phys. Fluids **22**, 105 (1979); D. Anderson, Phys. Rev. A **27**, 3135 (1983)
35. P. Sprangle, J.R. Peñano, B. Hafizi, Phys. Rev. E **66**, 046418 (2002)
36. S. Tzortzakis, L. Sudrie, M. Franco, B. Prade, A. Mysyrowicz, A. Couairon, L. Bergé, Phys. Rev. Lett. **87**, 213902 (2001)
37. L. Sudrie, A. Couairon, M. Franco, B. Lamouroux, B. Prade, S. Tzortzakis, A. Mysyrowicz, Phys. Rev. Lett. **89**, 186601 (2002)
38. P. Chernev, V. Petrov, Opt. Lett. **17**, 172 (1992)
39. J.E. Rothenberg, Opt. Lett. **17**, 583 (1992)
40. G.G. Luther, J.V. Moloney, A.C. Newell, E.M. Wright, Opt. Lett. **19**, 862 (1994)
41. S. Henz, J. Herrmann, Phys. Rev. E **53**, 4092 (1996)
42. N. Aközbek, C.M. Bowden, A. Talebpour, S. Chin, Phys. Rev. E **61**, 4540 (2000)
43. J. Schwarz, J.-C. Diels, Phys. Rev. A **65**, 013806 (2001)
44. Y.R. Shen, *The principles of nonlinear optics* (Wiley, New-York, 1984)
45. J.H. Marburger, Prog. Quant. Electr. **4**, 35 (1975)
46. H.R. Lange, G. Grillon, J.-F. Ripoche, M.A. Franco, B. Lamouroux, B.S. Prade, A. Mysyrowicz, Opt. Lett. **23**, 120 (1998)
47. M. Mlejnek, E.M. Wright, J.V. Moloney, IEEE J. Quant. Electron. **35**, 697 (1999)